Title
The Rate of NAD+ Breakdown Is Maintained Constant against Deletion or Overexpression of NAD+-Degrading Enzymes in Mammalian Cells

Author(s)
HARA Nobumasa / OSAGO Harumi / HIYOSHI Mineyoshi / MIURA Mikiko

Journal
Journal of nutritional science and vitaminology 70 (4) , 295 - 304

Published
2024-08-31

URL (The Version of Record)
https://doi.org/10.3177/jnsv.70.295

Vitaminology

The rate of NAD^+ breakdown is maintained constant against deletion or overexpression of NAD^+-degrading enzymes in mammalian cells

Nobumasa Hara[1], Harumi Osago, Mineyoshi Hiyoshi, and Mikiko Kobayashi-Miura

Department of Biochemistry, Shimane University Faculty of Medicine, 89-1, Izumo, Shimane 693-8501, Japan

Number of figures: 9

Running head: Compensatory regulation of cellular NAD^+ degradation

[1]To whom correspondence should be addressed: Department of Biochemistry, Shimane University Faculty of Medicine, 89-1, Izumo, Shimane 693-8501, Japan
Tel.: 81-853-20-2120; Fax: 81-853-20-2120; E-mail: nhara@med.shimane-u.ac.jp

Summary

Cellular NAD^+ is continuously degraded and synthesized under resting conditions. In mammals, NAD^+ synthesis is primarily initiated from nicotinamide (Nam) by Nam phosphoribosyltransferase, whereas poly (ADP-ribose) polymerase 1 (PARP1) and 2 (PARP2), sirtuin1 (SIRT1), CD38, and sterile alpha and TIR motif containing 1 (SARM1) are involved in NAD^+ breakdown. Using flux analysis with ^2H-labeled Nam, we found that when mammalian cells were cultured in the absence of Nam, cellular NAD^+ levels were maintained and NAD^+ breakdown was completely suppressed. In the presence of Nam, the rate of NAD^+ breakdown (R_B) did not significantly change upon PARP1, PARP2, SIRT1, or SARM1 deletion, whereas stable expression of CD38 did not increase R_B. However, R_B in PARP1-deleted cells was much higher compared with that in wild-type cells, in which PARP1 activity was blocked with a selective inhibitor. In contrast, R_B in CD38-overexpressing cells in the presence of a specific CD38 inhibitor was much lower compared with that in control cells. The results indicate that PARP1 deletion upregulates the activity of other NADases, whereas CD38 expression downregulates the activity of endogenous NADases, including PARP1 and PARP2. The rate of cellular NAD^+ breakdown and the resulting NAD^+ concentration may be maintained at a constant level, despite changes in the NAD^+-degrading enzyme expression, through the compensatory regulation of NADase activity.

Key words: NAD^+ breakdown, PARP1, PARP2, SIRT1, CD38, SARM1

Introduction

NAD^+ is a coenzyme involved in various cellular redox reactions. It is an essential component of metabolic pathways, including glycolysis, the citric acid cycle, and oxidative phosphorylation. NAD^+ also has important roles in energy metabolism, the circadian cycle, and aging through the function of the NAD^+-dependent deacetylases sirtuins (SIRTs) (*1-4*). Therefore, changes in cellular NAD^+ concentration ($[NAD^+]$) can have a significant impact on mammalian physiology, including humans.

Cellular NAD^+ is continuously synthesized and degraded under resting conditions (*5-7*). In mammals, NAD^+ synthesis is primarily initiated from nicotinamide (Nam) by the rate-limiting enzyme Nam phosphoribosyltransferase (Nampt) (*8*, *9*) (Fig. 1), whereas poly(ADP-ribose) polymerase 1 (PARP1) and 2 (PARP2), SIRT1, CD38, and sterile alpha and TIR motif containing 1 (SARM1) contribute to the breakdown of NAD^+ to Nam under the conditions (*10-13*) (Fig. 1).

Cellular NAD^+ levels are determined by the balance between its synthesis and breakdown. To understand the mechanisms regulating cellular $[NAD^+]$, quantitation of cellular $[NAD^+]$ alone is insufficient, thus determining the rates of synthesis (R_S) and breakdown (R_B) together with cellular $[NAD^+]$ is essential. We recently developed a method for the simultaneous quantitation of R_S and R_B together with cellular $[NAD^+]$ using mass spectrometry with ^2H (D)-labeled Nam (*6*). Based on this method, we compared R_S with R_B in various mammalian cells and found that R_S was nearly equal to R_B in all cells examined (6). Forced expression of Nampt resulted in a 6-fold increase in cellular Nampt activity, which increased R_S by only 2-fold, whereas R_B also increased by 2-fold, resulting in only a moderate increase in cellular $[NAD^+]$ (*6*). These observations indicate that R_S tends to remain constant during fluctuations of Nampt protein levels and

71 that NAD^+ synthesis from Nam is tightly associated with its breakdown. Therefore, a
72 specific molecular link must exist for the connection between NAD^+ synthesis and
73 breakdown, as previously reported (*6*). We hypothesized that the rate of cellular NAD^+
74 breakdown may also be kept constant against changes in the expression of NAD^+-
75 degrading enzymes.

76 In the present study, we measured R_B and R_S together with [NAD^+] in cultured
77 mammalian cells, in which PARP1, PARP2, SIRT1, CD38, and SARM1 were deleted or
78 overexpressed. These modifications did not induce obvious changes in R_B. Deletion of
79 PARP1 elevated [NAD^+] in 293T cells, but did not affect R_B. In contrast, overexpression
80 of CD38 decreased [NAD^+] without any observed increases in R_B. The absence of reduced
81 or increased rates of NAD^+ breakdown following PARP1 deletion or CD38
82 overexpression resulted from compensatory upregulation or downregulation, respectively,
83 of NAD^+-degrading enzyme activity. These results indicate that the rate of cellular NAD^+
84 breakdown remains constant, despite changes in the expression of NAD^+-degrading
85 enzymes.
86

Materials and Methods

Materials

[2, 4, 5, 6-D_4]Nam (d4-Nam) was purchased from CDN isotope (Quebec, Canada) and further purified by HPLC to remove contaminating d4-nicotinic acid (*6*). $^{13}C_6$-Nam and [ribose-$^{13}C_5$]NAD^+ were purchased from Cambridge Isotope Laboratories (Andover, MA, USA). Unlabeled Nam (d0-Nam), ABT-888, and CD38 inhibitor 1 (compound 78c) were purchased from FUJIFILM Wako Pure Chemical Corporation (Osaka, Japan), Enzo Life Science (Farmingdale, NY, USA), and Selleck Biotech (Osaka, Japan), respectively.

Cell culture

Rat hepatoma Fao (89042701) as well as the human cervical carcinoma HeLa (RCB0007), and embryonic kidney 293T (RCB2202) cell lines were obtained from ECACC (Salisbury, UK) and the Riken Cell Bank (Tsukuba, Japan), respectively, and maintained in Eagle's minimum essential medium (MEM, FUJIFILM Wako Pure Chemical Corporation) containing antibiotics and 10% fetal bovine serum (FBS). Fao, HeLa, and 293T cells were seeded at 3 x 10^5, 1.5 x 10^5, and 3 x 10^5 cells/well into collagen-coated (BD Biosciences, Bedford, MA, USA), CELLSTAR (Greiner Bio-One, Frickenhausen, Germany), and poly-D-lysine-coated (BD Biosciences) 12-well plates, respectively.

Generation of PARP1, PARP2, SIRT1, and SARM1 knockout (KO) cells

Deletion of PARP1, PARP2, SIRT1, or SARM1 was achieved by transfecting PARP1 (sc-400046), PARP2 (sc-402224), SIRT1 (sc-400085), or SARM1 (sc-403427) CRISPR/Cas9 KO plasmids (Santa Cruz Biotechnology, Dallas, TX, USA) encoding Cas9 nuclease and a PARP1, PARP2, SIRT1, or SARM1-specific 20-nt guide RNA into

293T cells. Dual PARP1 and PARP2 knockout was achieved by transfecting the PARP2 CRISPR/Cas9 KO plasmids into PARP1 KO cells. Deletion of both PARP1 and SIRT1 was achieved by transfecting the SIRT1 CRISPR/Cas9 KO plasmids into PARP1 KO cells. PARP1, PARP2, SIRT1, or SARM1 KO cells were confirmed by western blot analysis of PARP1, PARP2, SIRT1, or SARM1 expression.

Generation of CD38-expressing cells

293T cells were stably transfected with pCMV3-C-His-NCV empty vector (Sino Biological, Chesterbrook, PA, USA) or pCMV3-CD38-His (Sino Biological). Hygromycin-resistant (InvivoGen, San Diego, CA, USA) cell clones were isolated and clones expressing high levels of CD38 were selected by western blot analysis with antibodies raised against human CD38.

Inducible expression of SARM1

To achieve inducible expression of human SARM1 using the Tet-On system, the coding region of the enzyme was subcloned into the tetracycline-responsive element (TRE)-containing vector pTRE-Tight (Clontech, Mountain View, CA, USA). The resulting vector was transiently transfected using PolyFect transfection reagent (Qiagen, Hilden, Germany) into HeLa cells together with the pTet-On-Advanced vector (Clontech) as described previously (*6*). Expression was induced by the addition of doxycycline (Dox) to the culture medium.

Extraction of NAD^+ and Nam

To extract NAD^+ from the cells, 0.5 M perchloric acid (PCA) was added after the removal of the culture medium. The medium was mixed with one-tenth volume of 5 M PCA to precipitate the proteins. After centrifugation, the supernatants were collected, neutralized with 1 M ammonium formate containing internal standards ($^{13}C_6$-Nam and/or $^{13}C_5$-NAD^+), and subjected to LC/MS/MS analysis as described below.

PARP activation and CD38 ectoNADase assays

Cells were pre-cultured for 17 h with custom-made MEM without Nam (Nam-free MEM, Biological Industries, Beit, Haemek, Israel) containing 2 μM d0-Nam and 0.5% dialyzed FBS. To determine the effects of PARP1 and PARP2 activation on cellular NAD^+ levels, the cells were cultured for 3 h in 0.95 ml of the medium with or without 500 μM H_2O_2. Cellular NAD^+ levels were measured by LC/MS/MS. To determine CD38 ectoNADase activity, wild-type, empty vector-transfected control, and CD38-overexpressing 293T cells were cultured for 30 min in 0.8 ml of Nam-free MEM containing 10 μM NAD^+ and 0.5% dialyzed FBS. NAD^+ and its breakdown product, d0-Nam, in the medium were measured by LC/MS/MS.

Determination of R_S and R_B

After pre-culture for 17 h in Nam-free MEM containing 2 μM d0-Nam and 0.5% dialyzed FBS, the cells were cultured in a medium with d4-Nam replacing d0-Nam for 3 h. R_S and R_B were calculated as the amount of d3-NAD^+ newly appearing and decreasing unlabeled NAD^+ (d0-NAD^+) during the 3-h incubation, as described previously (*6*). Total cellular NAD^+ content was considered the sum of the amounts of d3-NAD^+ and d0-NAD^+. Because the amount of d0-NAD^+ degraded in the presence of 2 μM d4-Nam during

158 incubation was almost equal to that of d0-Nam released from the cells into the culture
159 medium (*6*), we also determined R_B from the amount of d0-Nam released.
160
161 *Cell counting and determination of cell volume*
162 Cell counting and determination of cell volume were done using an automated cell
163 counter, Scepter (Millipore, Billerica, MA, USA), as described previously (*6*). This
164 enabled the calculation of absolute values (μM/h) of R_S and R_B as well as cellular [NAD^+]
165 (μM). Cellular NAD^+ concentration was calculated from moles of NAD^+ in the cells and
166 their volumes measured.
167
168 *Western blot analysis*
169 To prepare cell lysates, SDS sample buffer was added directly to the cells after the
170 removal of the culture medium or to those collected by trypsinization. The lysates were
171 separated by SDS-PAGE, transferred onto Immobilon-P membranes (Millipore), and
172 blocked with 10% EzBlock Chemi (ATTO, Tokyo, Japan). The membranes were
173 incubated with anti-human PARP1 (Santa Cruz Biotechnology, sc-74469 or sc-8007),
174 PARP2 (Active Motif, Carlsbad, CA, USA, 39744), SIRT1 (Cell Signaling Technology,
175 Danvers, MA, USA, #8469), CD38 (Santa Cruz Biotechnology, sc-374650), or SARM1
176 (Novus Biologicals, Centennial, CO, USA, NBP2-29625SS) antibodies in Can Get Signal
177 Immunoreaction Enhancer Solution 1 (Toyobo, Osaka, Japan), followed by horseradish
178 peroxidase-conjugated goat anti-rabbit (MBL, Nagoya, Japan, #458) or anti-mouse IgG
179 antibodies (MBL, #330) in Can Get Signal Immunoreaction Enhancer Solution 2
180 (Toyobo). The bound antibodies were detected using Chemi-Lumi One Super (Nacalai
181 Tesque, Kyoto, Japan). Comparable loading of the proteins was confirmed using a rabbit

polyclonal anti-β-actin antibody (MBL, PM053).

LC/MS/MS

LC/MS/MS was performed using a Shimadzu HPLC system (Nexera X2, Shimadzu, Kyoto, Japan) connected to a triple quadrupole tandem mass spectrometer (LCMS-8030, Shimadzu) equipped with an ESI source operating in positive mode, as described previously (*6*). Briefly, NAD^+ and Nam were separated on Atlantis dC18 resin (150 x 2.1 mm i.d. column; 3-μm particle size; Waters, Milford, MA, USA) and detected in selected reaction monitoring (SRM) mode. The mobile phase consisted of 5 mM ammonium formate (solvent A) and methanol (solvent B). The percentage of solvent B was changed linearly as follows: 0 min, 2%; 3 min, 20%; 6 min, 70%; 11 min, 70%; 11.1 min, 2%; and 17 min, 2%. A calibration curve was generated for d0-NAD^+, d3-NAD^+, and d0-Nam using authentic standards and respective stable isotope-labeled internal standards ($^{13}C_5$-NAD^+ and $^{13}C_6$-Nam). The SRM transitions for d3-NAD^+, d0-NAD^+, d0-Nam, $^{13}C_5$-NAD^+, and $^{13}C_6$-Nam were 667 (precursor ion)/542 (product ion) or 667/136, 664/542 or 664/136, 123/80, 669/547, and 129/85, respectively. Shimadzu LabSolutions software (version 5.60SP2) was used for data acquisition and processing.

Statistical analysis

Data are presented as the mean ± SD. An unpaired, two-tailed Student's *t*-test was used for two group comparisons. One-way ANOVA with Tukey's post-hoc test was used for comparisons of three or more groups. Asterisks displayed in the figure denote statistical significance. $P < 0.05$ was considered statistically significant.

Results

Cellular NAD^+ is degraded only in the presence of Nam

Fao, HeLa, and 293T cells were incubated with or without 2 μM d4-Nam in Nam-free MEM. R_S, R_B, and cellular [NAD^+] were measured under resting conditions. As shown in Fig. 2, cellular NAD^+ levels were maintained in the absence of Nam, and breakdown of cellular NAD^+ was not observed under the conditions (Fig. 2). In contrast, when Nam was added to the cells, NAD^+ breakdown was observed and R_B was nearly equal to R_S (Fig. 2). These results indicate that cellular NAD^+ is degraded only in the presence of the Nampt substrate Nam, and support the existence of a molecular link connecting the synthesis of NAD^+ to its breakdown (*6*).

Effects of SARM1 deletion and overexpression on R_B

SARM1 is an NADase with a prodegenerative role in programmed axon death (*12*). It is activated by NAD^+ synthetic enzyme Nampt reaction product Nam mononucleotide (NMN) (*14*, *15*). We hypothesized that SARM1 may connect NAD^+ synthesis to its breakdown under resting conditions; thus, we determined R_B in SARM1 KO cells. Loss of SARM1 in 293T cells (Fig. 3A) did not affect R_S or cellular [NAD^+], whereas only a small decrease in R_B (12%) was observed in the KO cells (Fig. 3B). To further examine a potential role for SARM1 in NAD^+ breakdown, we overexpressed SARM1 using a Dox-inducible gene expression system (*6*) in HeLa cells, which do not express a significant amount of endogenous SARM1 (Fig. 3C). As shown in Fig. 3D, the induced expression of SARM1 did not affect R_B, R_S, or cellular [NAD^+]. Taken together, the results indicate that SARM1 may not mediate the breakdown of NAD^+ under resting conditions.

Deletion of PARP1 and/or PARP2 does not decrease R_B

To determine the potential role of PARP1 and PARP2 in NAD^+ breakdown under resting conditions, we generated PARP1 and/or PARP2 KO cells (Fig. 4A, B) and measured R_S, R_B, and cellular [NAD^+]. Western blot analysis confirmed the absence of PARP1 and/or PARP2 in the KO cells (Fig. 4A). The absence of PARP1 was further confirmed by subjecting KO cells to DNA damage with H_2O_2 to hyperactivate PARP1 and PARP2 (*16*). As shown in Fig. 4B, the loss of PARP1, but not PARP2, almost completely prevented the depletion of NAD^+ in DNA-damaged cells, which is consistent with the major role of PARP1 in DNA damage-induced cellular NAD^+ depletion (*17*).

In PARP1 KO cells, breakdown of NAD^+ was still observed under resting conditions (Fig. 4C). Loss of PARP1 did not induce a statistically significant decrease in R_B; rather, there was a trend of increased R_B ($P = 0.114$) and R_S ($P = 0.123$) in PARP1 KO cells compared with wild-type (WT) cells (Fig. 4C). PARP2 KO or PARP1 and PARP2 double KO did not decrease R_B (Fig. 4C). As shown in Fig. 4C, loss of PARP1, but not PARP2, significantly increased cellular [NAD^+] by ~30%, which is consistent with previous reports (*18*, *19*). In the absence of PARP1, the expression of PARP2 (Figs. 4A and 5A), SIRT1 (Fig. 5A), or CD38 (Fig. 5A) protein was unchanged.

Deletion of SIRT1 does not decrease R_B

Next, we determined the role of SIRT1 in NAD^+ breakdown under resting conditions. SIRT1 KO cells (Fig. 5A) were generated and R_S, R_B, and cellular [NAD^+] were measured. The loss of SIRT1 did not affect R_S, R_B, or cellular [NAD^+] (Fig. 5B). Deletion of SIRT1 in PARP1 KO cells did not further affect R_B or R_S. Loss of PARP1 together with or without SIRT1 increased cellular [NAD^+] by 25% under these conditions (Fig. 5B).

254

255 **Overexpression of CD38 does not increase R_B**

256 Consistent with previous reports (*19*, *20*), WT 293T cells did not express a significant
257 amount of ectoNADase CD38 (Figs. 5A and 6A), and we did not detect ectoNADase
258 activity in the cells. When the cells were cultured in a medium containing NAD^+, the
259 added NAD^+ was not degraded (Fig. 6B). These results indicate that CD38 does not
260 mediate NAD^+ breakdown under resting conditions.

261 To further examine the effect of CD38 on cellular NAD^+ breakdown, we stably
262 overexpressed CD38 and determined R_B in the CD38-overexpressing cells. In marked
263 contrast with control cells transfected with an empty vector, CD38 plasmid transfection
264 yielded high CD38 protein expression (Fig. 6A) and high ectoNADase activity (Fig. 6B),
265 thus confirming enzymatically active CD38 expression; however, forced expression of
266 CD38 did not increase R_B (Fig. 6C). CD38 expression significantly decreased cellular
267 [NAD^+] (Fig. 6C), which is consistent with that of previous reports (*19-21*). Upon CD38
268 overexpression, the expression of PARP1, PARP2, or SIRT1 protein was unchanged (Fig.
269 6D).

270

271 **Effects of the pharmacological inhibition of PARP1 and PARP2 on R_B**

272 The effects of pharmacological inhibition of NAD^+-degrading enzymes on R_B were
273 determined. First, the effect of a selective inhibitor of PARP1 and PARP2, ABT-888 (*22*),
274 on R_B in WT and PARP1 KO cells was determined. In the presence of 50 nM ABT-888,
275 the concentration required for complete inhibition of PARP1and PARP2 (*22*), R_B
276 decreased by 44% in WT cells (Fig. 7A), indicating the involvement of PARP1 and
277 PARP2 in NAD^+ breakdown as well as other enzymes for the remaining NAD^+

consumption. In contrast, in PARP1 KO cells, R_B was unchanged in the presence of 50 nM ABT-888 (Fig. 7A), indicating that not only PARP1, but also PARP2, could not be responsible for NAD^+ breakdown in the KO cells. Importantly, R_B in PARP1 KO cells was 1.8 times higher compared with that observed in WT cells in the presence of the inhibitor (Fig. 7B). These observations indicate upregulation of the activity of other NADases in the absence of PARP1, which results in no net change in R_B. Cellular NAD^+ levels were elevated in the presence of ABT-888 in WT, but not PARP1 KO, cells (Fig. 7A, B).

Effects of the pharmacological inhibition of CD38 on R_B

Next, the effect of a specific inhibitor of CD38, compound 78c (*23*), on R_B in CD38-overexpressing cells was determined. In CD38-overexpressing cells, R_B was decreased by 25% with compound 78c in a dose-dependent manner, indicating that CD38 activity accounts for 25% of R_B in the cells under resting conditions and that other enzymes are responsible for the remaining NAD^+ consumption (Fig. 8A). In contrast, in empty vector-transfected control cells, R_B was not decreased following treatment with the CD38 inhibitor (Fig. 8A), thus confirming no involvement of CD38 in NAD^+ breakdown in the control cells. R_B in CD38-overexpressing cells in the presence of the inhibitor was considerably lower compared with that in the control cells (Fig. 8B). This indicates reduced activity of endogenous NADases upon CD38 overexpression, resulting in no net change in R_B. Cellular NAD^+ levels were elevated in the presence of the inhibitor in CD38-overexpressing, but not the control, cells (Fig. 8A, B). To determine whether PARP1 and PARP2 activity is reduced in the presence of CD38, we examined the effects of ABT-888 on R_B in CD38-overexpressing cells. Although ABT-888 significantly

302 decreased R_B (Fig. 8C), it was significantly less effective on R_B in CD38-overexpressing
303 cells compared with control cells (Fig. 8D). These results indicate that the activity of
304 PARP1 and PARP2 is decreased in the presence of CD38, and CD38 expression reduces
305 the activity of endogenous NADases.

306 **Discussion**

307 NAD^+ is continuously degraded and synthesized under resting conditions in
308 mammalian cells (*5*-*7*). In the present study, we deleted or overexpressed the NAD^+-
309 degrading enzymes, PARP1, PARP2, SIRT1, CD38, and SARM1, and determined R_B in
310 the modified cells; however, these modifications did not induce obvious changes in R_B.
311 In contrast, experiments with pharmacological inhibitors revealed that the activity of
312 other NADases was upregulated in response to PARP1 deletion, whereas CD38
313 expression reduced the activity of endogenous NADases, as summarized in Fig. 9. The
314 total cellular NAD^+-degrading activity may be kept constant against changes in the
315 expression of NAD^+-degrading enzymes.

316 In the present study, we demonstrated that cellular NAD^+ is degraded only in the
317 presence of the Nampt substrate Nam and that R_B is almost equal to R_S under these
318 conditions. This supports the existence of a specific molecular link connecting the
319 synthesis of NAD^+ to its breakdown (*6*). Because SARM1 is activated by the Nampt
320 reaction product NMN (*14*, *15*), we hypothesized that SARM1 may connect NAD^+
321 synthesis to its breakdown; however, the loss of SARM1 induced only a small decrease
322 in R_B, whereas SARM1 overexpression did not increase R_B. Taken together, SARM1 may
323 not mediate NAD^+ breakdown, thus the molecular link remains unknown.

324 Although PARP1 is believed to be one of the major NAD^+-degrading enzymes
325 under resting conditions (*17*, *18*), whether its deletion decreases R_B remains to be
326 determined. In the present study, we did not observe a decrease in R_B upon PARP1
327 deletion. In contrast, when PARP1 and PARP2 activity was inhibited with ABT-888, we
328 observed decreased R_B in WT cells, indicating the involvement of the PARPs in NAD^+
329 breakdown. Consistent with this result, Liu *et al*. also reported that PARP1 and PARP2

330 account for one-third of NAD^+ breakdown using an inhibitor under resting conditions in
331 T47D breast cancer cells (*5*). In the present study, we found that R_B in PARP1 KO cells
332 was much higher compared with that in WT cells in the presence of ABT-888. Thus, we
333 demonstrated the upregulation of the activity of other NADases in the absence of PARP1
334 (Fig. 9). It is likely that the loss of PARP1 activity and the induction of the activity of
335 other NADases resulted in no observed decrease in R_B. Western blot analysis excluded
336 the increased expression of PARP2, SIRT1, or CD38 in the absence of PARP1.
337 CD38 is also believed to be a major NAD^+-degrading enzyme under resting
338 conditions (*19*-*21*, *24*), but whether changing CD38 expression levels alters R_B remains
339 to be determined. Consistent with previous studies (*19*, *20*), we observed the absence of
340 CD38 in WT 293T cells; however, stable expression of CD38 did not increase R_B. Using
341 a specific inhibitor of CD38, compound 78c, we found that in the presence of the inhibitor,
342 R_B in CD38-overexpressing cells was significantly lower compared with that in WT cells,
343 demonstrating suppression of endogenous NADase activity associated with its expression
344 (Fig. 9). Similar to PARP1 KO cells, but in an opposite manner, increased CD38 activity
345 and downregulation of endogenous NADase activity may not result in increased R_B upon
346 induction of CD38 expression. Although we did not fully identify the suppressed
347 NADases, a much smaller effect of ABT-888 on R_B in CD38-overexpressing cells
348 compared with control cells indicates that NADases with suppressed activity include
349 PARP1 and PARP2, and that CD38 expression suppresses endogenous NADases.
350 We observed that SIRT1 KO did not change R_B in 293T cells. Using small-
351 molecule inhibitors, SIRT1 and SIRT2 were shown to degrade cellular NAD^+ under
352 resting conditions in T47D cell lines (*5*). Whether SIRT1 deletion induces the activity of
353 other NADase(s), as in the case of PARP-1 deletion, remains to be determined.

In the present study, without significant changes in R_S and R_B, cellular [NAD^+] was increased in PARP1KO and PARP1 and PARP2 double KO cells whereas CD38 expression decreased cellular [NAD^+]. In these modified cells, we did not determine metabolites in the kynurenine pathway (*13*) and expression of the enzymes in the pathway. Thus, whether the activation or inhibition of NAD^+ synthesis through the pathway is involved in the observed changes in cellular [NAD^+] remains unknown.

In conclusion, NAD^+ breakdown is tightly connected to its synthesis under resting conditions. Thus, cellular NAD^+ is not degraded when NAD^+ is not synthesized. R_B is not altered by the deletion or overexpression of known NAD^+-degrading enzymes. No observed changes in R_B are, at least in part, the result of the compensatory regulation of cellular NAD^+ breakdown. Upon PARP1 deletion, the activity of other NADases is upregulated, whereas enhanced expression of CD38 reduces the activity of other endogenous NADases. The upregulation of cellular NAD^+-degrading activity may maintain a high turnover rate of cellular NAD^+ to maintain cellular [NAD^+] at constant levels, whereas downregulation of NAD^+-degrading activity may prevent excessive decreases in NAD^+ levels. R_S also tends to be held constant against fluctuation of Nampt protein levels through the inhibition of Nampt by cellular NAD^+ (*6*). Not only cellular NAD^+-synthesizing, but also its degrading activity, may be kept constant against changes in the expression of the enzymes involved. The molecular mechanism underlying the compensatory regulation of cellular NAD^+ breakdown as well as the molecular basis of the tight connection between NAD^+ synthesis and breakdown, including a linker mediating the connection, remains unclear. Elucidation of these mechanisms may provide insight into the homeostasis of cellular NAD^+ concentrations and an important clue toward an NAD^+ boosting strategy (*11*).

Authorship

Research conception and design: NH; experiments: NH and HO; statistical analysis of the data: MH; interpretation of the data: NH, HO, MH, and MK; writing of the manuscript: NH.

Disclosure of the state of COI

No conflicts of interest to declare.

Acknowledgments

This study was supported by JSPS KAKENHI Grant Numbers JP18K11072 and JP 21K11696. We are grateful to Mikako Tsuchiya for the helpful discussion.

References

1) Schug TT, Li X. 2011. Sirtuin 1 in lipid metabolism and obesity. *Ann Med* **43**: 198-211.

2) Guarente L. 2011. Franklin H. Epstein Lecture: Sirtuins, aging, and medicine. *N Engl J Med* **364**: 2235-2244.

3) Hall JA, Dominy JE, Lee Y, Puigserver P. 2013. The sirtuin family's role in aging and age-associated pathologies. *J Clin Invest* **123**: 973-979.

4) Imai S, Guarente L. 2014. NAD^+ and sirtuins in aging and disease. *Trends Cell Biol* **24**: 464-471.

5) Liu L, Su X, Quinn WJ 3rd, Hui S, Krukenberg K, Frederick DW, Redpath P, Zhan L, Chellappa K, White E, Migaud M, Mitchison TJ, Baur JA, Rabinowitz JD. 2018. Quantitative analysis of NAD synthesis-breakdown fluxes. *Cell Metab* **27**: 1067-1080.

6) Hara N, Osago H, Hiyoshi M, Kobayashi-Miura M, Tsuchiya M. 2019. Quantitative analysis of the effects of nicotinamide phosphoribosyltransferase induction on the rates of NAD^+ synthesis and breakdown in mammalian cells using stable isotope-labeling combined with mass spectrometry. *PLoS One* **14**: e0214000.

7) McReynolds MR, Chellappa K, Chiles E, Jankowski C, Shen Y, Chen L, Descamps HC, Mukherjee S, Bhat YR, Lingala SR, Chu Q, Botolin P, Hayat F, Doke T, Susztak K, Thaiss CA, Lu W, Migaud ME, Su X, Rabinowitz JD, Baur JA. 2021. NAD^+ flux is maintained in aged mice despite lower tissue concentrations. *Cell Syst* **12**: 1160-1172.

8) Chiarugi A, Dölle C, Felici R, Ziegler M. 2012. The NAD metabolome--a key determinant of cancer cell biology. *Nat Rev Cancer* **12**: 741-752.

9) Garten A, Schuster S, Penke M, Gorski T, de Giorgis T, Kiess W. 2015. Physiological and pathophysiological roles of NAMPT and NAD metabolism. *Nat Rev Endocrinol* **11**: 535-546.

414 *10*) Cantó C, Menzies KJ, Auwerx J. 2015. NAD^+ metabolism and the control of energy
415 homeostasis: A balancing act between mitochondria and the nucleus. *Cell Metab* **22**:
416 31-53.
417 *11*) Rajman L, Chwalek K, Sinclair DA. 2018. Therapeutic potential of NAD-boosting
418 molecules: The in vivo evidence. *Cell Metab* **27**: 529-547.
419 *12*) Loring HS, Thompson PR. 2020. Emergence of SARM1 as a potential therapeutic
420 target for Wallerian-type diseases. *Cell Chem Biol* **27**: 1-13.
421 *13*) Covarrubias AJ, Perrone R, Grozio A, Verdin E. 2021. NAD^+ metabolism and its roles
422 in cellular processes during ageing. *Nat Rev Mol Cell Biol* **22**: 119-141.
423 *14*) Zhao ZY, Xie XJ, Li WH, Liu J, Chen Z, Zhang B, Li T, Li SL, Lu JG, Zhang L,
424 Zhang LH, Xu Z, Lee HC, Zhao YJ. 2019. A cell-permeant mimetic of NMN activates
425 SARM1 to produce cyclic ADP-ribose and induce non-apoptotic cell death. *iScience*
426 **15**: 452-466.
427 *15*) Figley MD, Gu W, Nanson JD, Shi Y, Sasaki Y, Cunnea K, Malde AK, Jia X, Luo Z,
428 Saikot FK, Mosaiab T, Masic V, Holt S, Hartley-Tassell L, McGuinness HY, Manik
429 MK, Bosanac T, Landsberg MJ, Kerry PS, Mobli M, Hughes RO, Milbrandt J, Kobe
430 B, DiAntonio A, Ve T. 2021. SARM1 is a metabolic sensor activated by an increased
431 NMN/NAD^+ ratio to trigger axon degeneration. *Neuron* **109**: 1118-1136.
432 *16*) Schraufstatter IU, Hinshaw DB, Hyslop PA, Spragg RG, Cochrane CG. 1986. Oxidant
433 injury of cells. DNA strand-breaks activate polyadenosine diphosphate-ribose
434 polymerase and lead to depletion of nicotinamide adenine dinucleotide. *J Clin Invest*
435 **77**: 1312-1320.
436 *17*) Bai P, Cantó C. 2012. The role of PARP-1 and PARP-2 enzymes in metabolic
437 regulation and disease. *Cell Metab* **16**: 290-295.

438 *18*) Bai P, Cantó C, Oudart H, Brunyánszki A, Cen Y, Thomas C, Yamamoto H, Huber A,
439 Kiss B, Houtkooper RH, Schoonjans K, Schreiber V, Sauve AA, Menissier-de Murcia
440 J, Auwerx J. 2011. PARP-1 inhibition increases mitochondrial metabolism through
441 SIRT1 activation. *Cell Metab* **13**: 461-468.
442 *19*) Camacho-Pereira J, Tarragó MG, Chini CCS, Nin V, Escande C, Warner GM, Puranik
443 AS, Schoon RA, Reid JM, Galina A, Chini EN. 2016. CD38 dictates age-related NAD
444 decline and mitochondrial dysfunction through an SIRT3-dependent mechanism. *Cell*
445 *Metab* **23**: 1127-1139.
446 *20*) Escande C, Nin V, Price NL, Capellini V, Gomes AP, Barbosa MT, O'Neil L, White
447 TA, Sinclair DA, Chini EN. 2013. Flavonoid apigenin is an inhibitor of the NAD^+ase
448 CD38: implications for cellular NAD^+ metabolism, protein acetylation, and treatment
449 of metabolic syndrome. *Diabetes* **62**: 1084-1093.
450 *21*) Chini CCS, Peclat TR, Warner GM, Kashyap S, Espindola-Netto JM, de Oliveira GC,
451 Gomez LS, Hogan KA, Tarragó MG, Puranik AS, Agorrody G, Thompson KL, Dang
452 K, Clarke S, Childs BG, Kanamori KS, Witte MA, Vidal P, Kirkland AL, De Cecco
453 M, Chellappa K, McReynolds MR, Jankowski C, Tchkonia T, Kirkland JL, Sedivy
454 JM, van Deursen JM, Baker DJ, van Schooten W, Rabinowitz JD, Baur JA, Chini EN.
455 2020. CD38 ecto-enzyme in immune cells is induced during aging and regulates
456 NAD^+ and NMN levels. *Nat Metab* **2**: 1284-1304.
457 *22*) Thorsell AG, Ekblad T, Karlberg T, Löw M, Pinto AF, Trésaugues L, Moche M, Cohen
458 MS, Schüler H. 2017. Structural basis for potency and promiscuity in poly(ADP-
459 ribose) polymerase (PARP) and tankyrase inhibitors. *J Med Chem* **60**: 1262-1271.
460 *23*) Tarragó MG, Chini CCS, Kanamori KS, Warner GM, Caride A, de Oliveira GC, Rud
461 M, Samani A, Hein KZ, Huang R, Jurk D, Cho DS, Boslett JJ, Miller JD, Zweier JL,

462 Passos JF, Doles JD, Becherer DJ, Chini EN. 2018. A potent and specific CD38
463 inhibitor ameliorates age-related metabolic dysfunction by reversing tissue
464 NAD^+ decline. *Cell Metab* **27**: 1081-1095.
465 *24*) Aksoy P, White TA, Thompson M, Chini EN. 2006. Regulation of intracellular levels
466 of NAD: a novel role for CD38. *Biochem Biophys Res Commun* **345**: 1386-1392.

467 **Figure legends**

468

469 Fig. 1. Metabolic pathway for the salvage NAD^+ synthesis and NAD^+-degrading enzymes
470 in mammals. NMN, Nam mononucleotide; NMNATs, NMN adenylyltransferases.

471

472 Fig. 2. NAD^+ breakdown in the presence or absence of Nam. Fao, HeLa, and 293T cells
473 were cultured in d0-Nam-free MEM with or without 2 μM d4-Nam. R_B and R_S were
474 measured based on d0-Nam released into the medium and d3-NAD^+ synthesized in cells,
475 respectively, together with cellular [NAD^+]. Data shown represent the mean ± S.D. of
476 three separate experiments. Asterisks indicate significant differences (*$P < 0.05$, ***$P <$
477 0.001).

478

479 Fig. 3. Effects of SARM1 KO and overexpression on R_S, R_B, and cellular [NAD^+]. A:
480 Protein expression of SARM1 and β-actin in wild-type (WT, clones NT and #8) and
481 SARM1 KO (SARM1 KO, clones #41, #30, and #27) 293T cells. Representative of three
482 separate experiments. NT, non-transfected. B: R_S, R_B, and cellular [NAD^+] in WT and
483 SARM1 KO cells. Data shown represent the mean ± S.D. of six and nine separate
484 experiments for WT and SARM1 KO cells, respectively. An asterisk indicates a
485 significant difference (*$P < 0.05$). C, D: SARM1 expression was induced in HeLa cells
486 in the presence of 1 μM Dox. Protein expression of SARM1 and β-actin (C).
487 Representative of three separate experiments. R_S, R_B, and cellular [NAD^+] in WT and
488 SARM1-overexpressing cells (D). Data shown represent the mean ± S.D. of three separate
489 experiments. Treatment of HeLa cells with the same concentration of Dox without
490 transfection does not affect R_S, R_B, or cellular [NAD^+] (*6*) and when HeLa cells

transfected with empty vector are treated with or without Dox, R_S, R_B, and cellular [NAD^+] are similar to those in non-transfected cells without Dox (*6*).

Fig. 4. Effects of PARP1 and/or PARP2 KO on R_S, R_B, and cellular [NAD^+]. A: Expression of PARP1, PARP2, and β-actin protein in wild-type, PARP1 KO, PARP2 KO, and PARP1 and PARP2 double KO (WT, 1KO, 2KO, and DKO, respectively) 293T cells. Representative of four separate experiments. NT, non-transfected. B: [NAD^+] in WT, 1KO, 2KO, and DKO cells with or without H_2O_2. Data shown represent the mean ± S.D. of four separate experiments. Asterisks indicate significant differences (***$P < 0.001$). C: R_S, R_B, and [NAD^+] determined in WT, 1KO, 2KO, and DKO cells. Data shown represent the mean ± S.D. of eight separate experiments. Asterisks indicate significant differences (*$P < 0.05$, **$P < 0.01$).

Fig. 5. Effects of PARP1 and/or SIRT1 KO on R_S, R_B, and cellular [NAD^+]. A: Expression of PARP1, SIRT1, PARP2, CD38, and β-actin protein in wild-type, PARP1 KO, SIRT1 KO, and PARP1 and SIRT1 double KO (WT, PARP1 KO, SIRT1 KO, and DKO, respectively) 293T cells. Representative of five separate experiments. NT, non-transfected; CD38OE, CD38-overexpressing cells (see Fig. 6) were used as a positive control for detecting CD38 expression. B: R_S, R_B, and [NAD^+] determined in WT, PARP1 KO, SIRT1 KO, and DKO cells. Data shown represent the mean ± S.D. of ten separate experiments. Asterisks indicate significant differences (*$P < 0.05$, **$P < 0.01$).

Fig. 6. Effects of CD38 overexpression on R_S, R_B, and cellular [NAD^+]. 293T cells were stably transfected with empty vector (EV) or CD38 plasmid. A: Expression of CD38 and

β-actin protein in wild-type (WT), EV-transfected control (clones C3 and C7), and CD38-overexpressing (CD38OE, clones #4 and #6) cells. Representative of four separate experiments. B: EctoNADase activity of WT cells and clones C3, C7, #4, and #6. Cells were cultured with Nam-free MEM containing NAD^+. Nam produced in the medium during the incubation was measured. Data shown represent the mean ± S.D. of four separate experiments. Asterisks indicate significant differences (***$P < 0.001$). C: R_S, R_B, and [NAD^+] determined in WT, the control (C), and CD38-overexpressing (CD38OE) cells. Data shown represent the mean ± S.D. of four and eight separate experiments for WT, and the control and CD38OE cells, respectively. Asterisks indicate significant differences (*$P < 0.05$, **$P < 0.01$). D: Expression of PARP1, SIRT1, PARP2, CD38, and β-actin protein in the control (clone C7) and CD38OE (clones #4 and #6) cells.

Fig. 7. Effects of PARP inhibitor ABT-888 on R_B and cellular [NAD^+].

WT and PARP1 KO (clones #5 and #C30) 293T cells were cultured in d0-Nam-free MEM supplemented with d4-Nam in the presence of the indicated concentrations of ABT-888. R_B was determined from d0-Nam released into the medium during the incubation. A: Effects of ABT-888 on R_B and cellular [NAD^+]. B: Replot of data in (A). Data shown represent the mean ± S.D. of four and eight separate experiments for WT and PARP1 KO cells, respectively. Asterisks indicate significant differences (*$P < 0.05$, **$P < 0.01$, ***$P < 0.001$).

Fig. 8. Effects of compound 78c and ABT-888 on R_B and cellular [NAD^+].

Empty vector-transfected control (EV, clone C7) and CD38-overexpressing (CD38, clones #4 and #6) 293T cells were cultured in d0-Nam-free MEM supplemented with d4-

539 Nam in the presence of the indicated concentrations of DMSO, compound 78c (78c), and
540 ABT-888. R_B was determined from d0-Nam released into the medium during the
541 incubation. A: Effects of compound 78c on R_B and cellular [NAD^+]. B: Replot of data in
542 (A). C: Effects of ABT-888 on R_B and cellular [NAD^+]. D: Replot of data in (C). Data
543 shown represent the mean ± S.D. of four and eight separate experiments for the control
544 and CD38-overexpressing cells, respectively. Asterisks indicate significant differences
545 (*$P < 0.05$, **$P < 0.01$, ***$P < 0.001$).
546
547 Fig. 9. Summary of the compensatory regulation of cellular NAD^+-degrading activity.
548 R_B in PARP1-deleted cells (PARP1 KO) is markedly higher compared with that in the
549 wild-type cells (WT), in which the activity of PARP1 and PARP2 was blocked with the
550 selective inhibitor ABT-888. In contrast, R_B in CD38-overexpressing cells (CD38) in the
551 presence of the specific CD38 inhibitor, compound 78c, was much lower compared with
552 that in the empty vector-transfected control cells (EV). PARP1 deletion upregulates the
553 activity of other NADases, whereas the expression of CD38 reduces the activity of
554 endogenous NADases, including PARP1 and PARP2. The data shown are from Figs. 7
555 and 8.
556
557
558
559
560
561
562

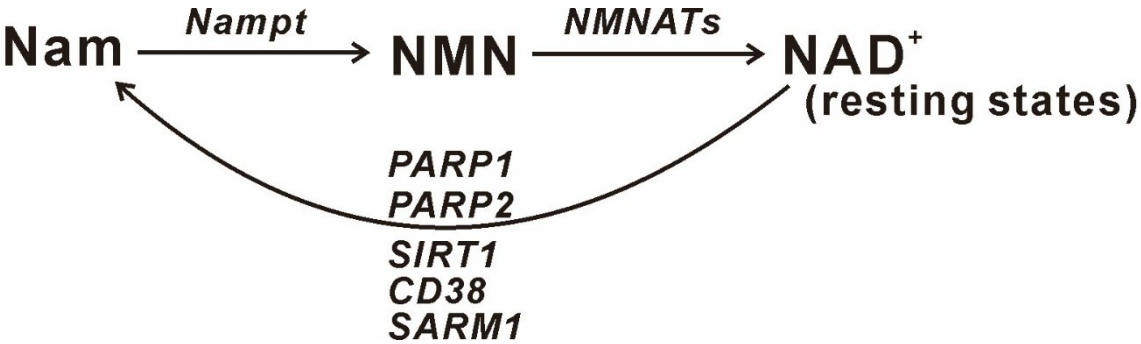
Nam
Nampt
NMN
NMNATs
NAD+
(resting states)
PARP1
PARP2
SIRT1
CD38
SARM1

Figure 1

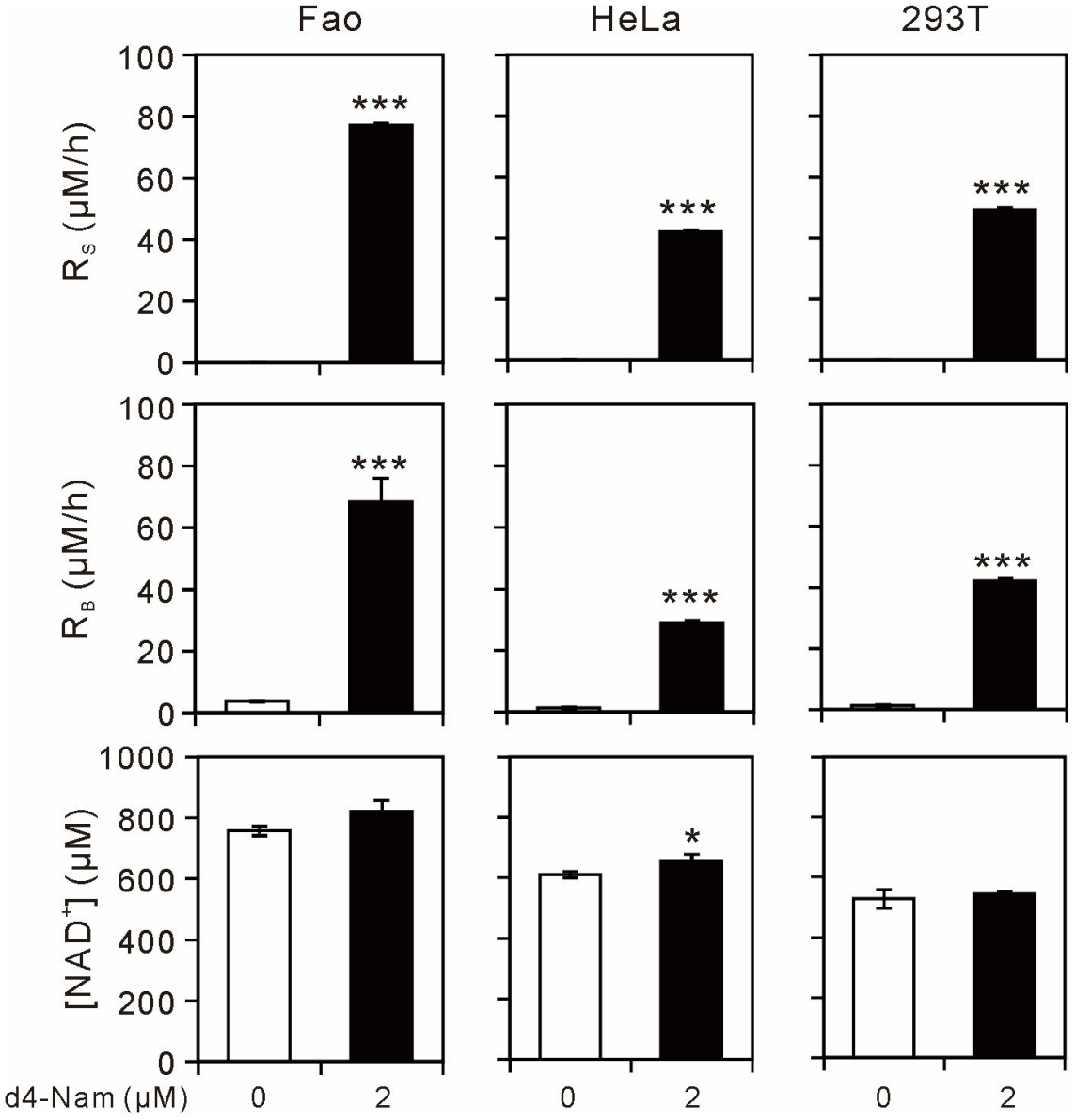

Figure 2

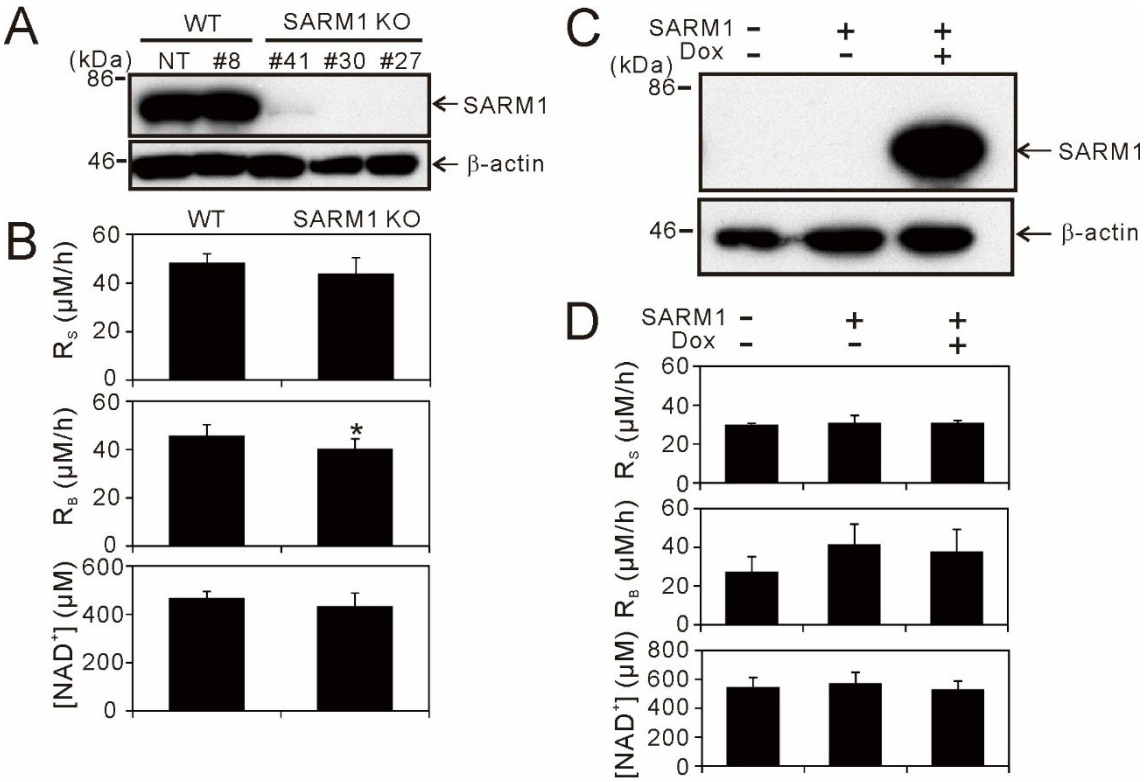
A
WT
SARM1 KO
(kDa)
NT
#8
#41
#30
#27
86
46
SARM1
β-actin
B
WT
SARM1 KO
R_S (μM/h)
R_B (μM/h)
[NAD+] (μM)
*
C
SARM1
Dox
(kDa)
86
46
SARM1
β-actin
D
SARM1
Dox
R_S (μM/h)
R_B (μM/h)
[NAD+] (μM)

Figure 3

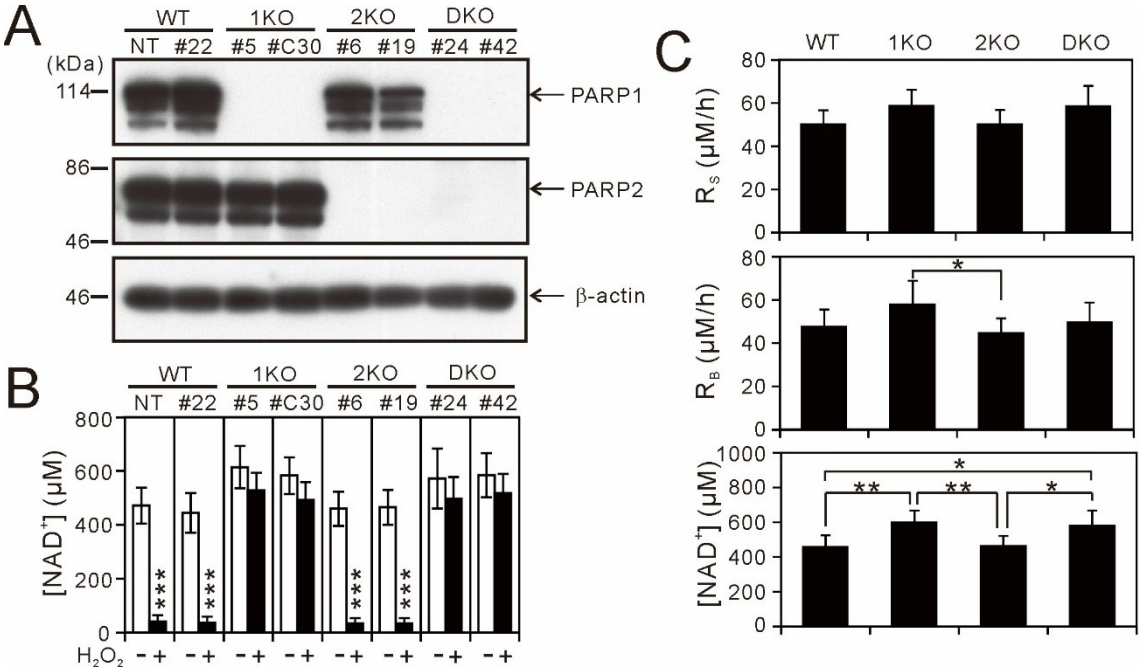
A
WT
1KO
2KO
DKO
NT #22 #5 #C30 #6 #19 #24 #42
(kDa)
114
PARP1
86
PARP2
46
46
β-actin
B
[NAD+] (μM)
H2O2 - + - + - + - + - + - + - + - +
C
RS (μM/h)
RB (μM/h)
[NAD+] (μM)

Figure 4

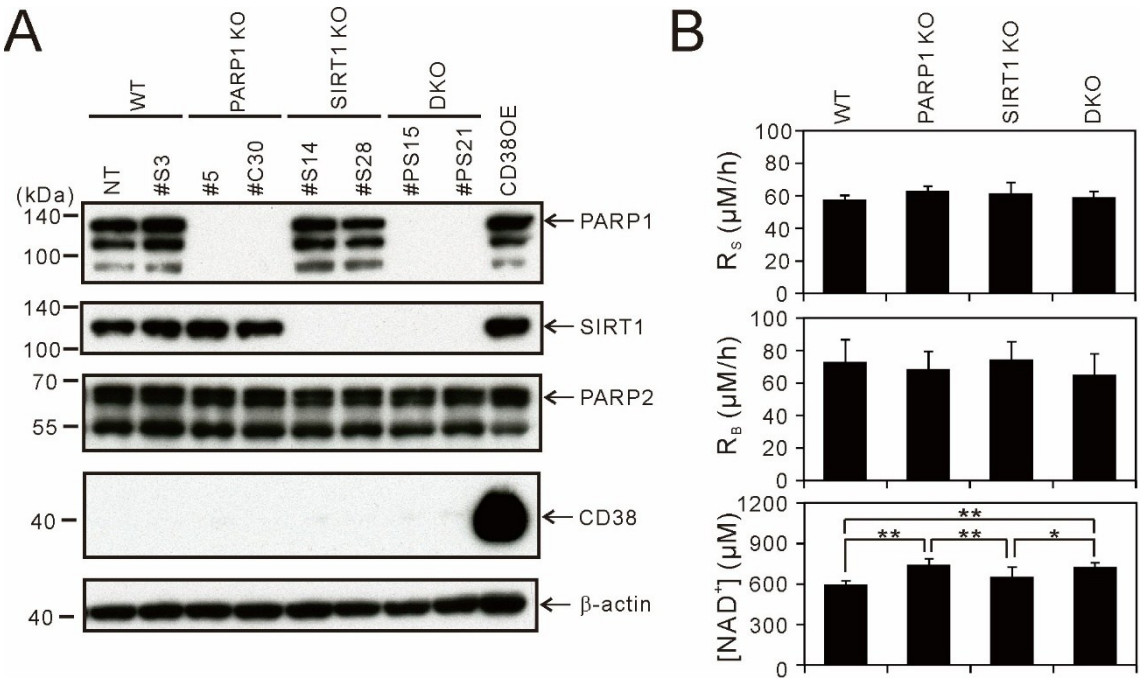
A
WT
PARP1 KO
SIRT1 KO
DKO
NT
#S3
#5
#C30
#S14
#S28
#PS15
#PS21
CD38OE
(kDa)
140
100
PARP1
140
100
SIRT1
70
55
PARP2
40
CD38
40
β-actin
B
WT
PARP1 KO
SIRT1 KO
DKO
R_S (μM/h)
R_B (μM/h)
[NAD+] (μM)
**
**
**
*

Figure 5

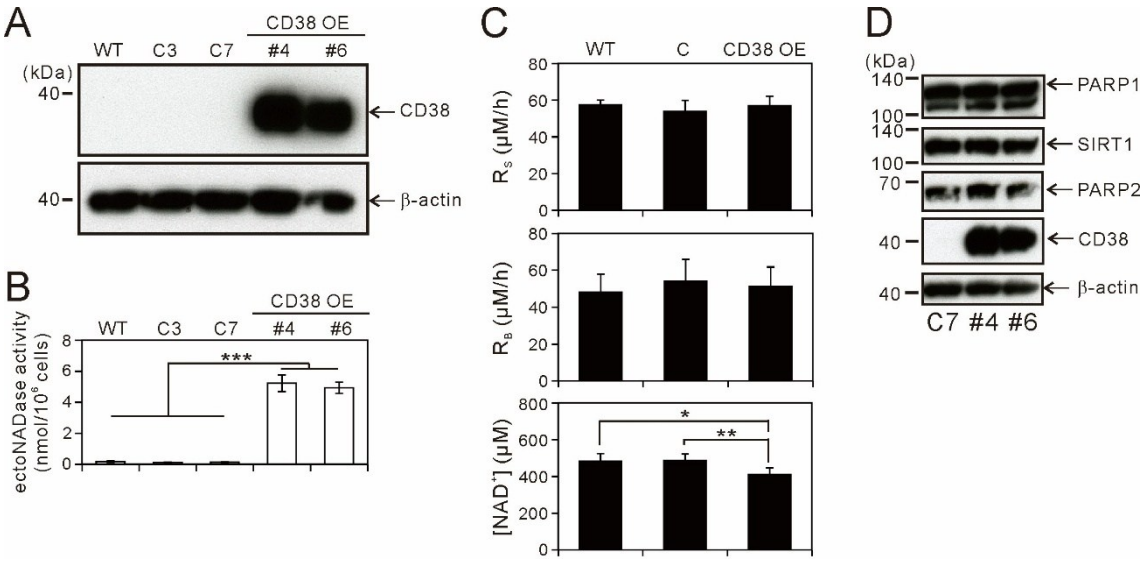
A
CD38 OE
WT C3 C7 #4 #6
(kDa)
40
CD38
40
β-actin
B
CD38 OE
WT C3 C7 #4 #6
ectoNADase activity (nmol/10^6 cells)
***
C
WT C CD38 OE
R_S (μM/h)
R_B (μM/h)
[NAD+] (μM)
*
**
D
(kDa)
140
PARP1
100
140
SIRT1
100
70
PARP2
40
CD38
40
β-actin
C7 #4 #6

Figure 6

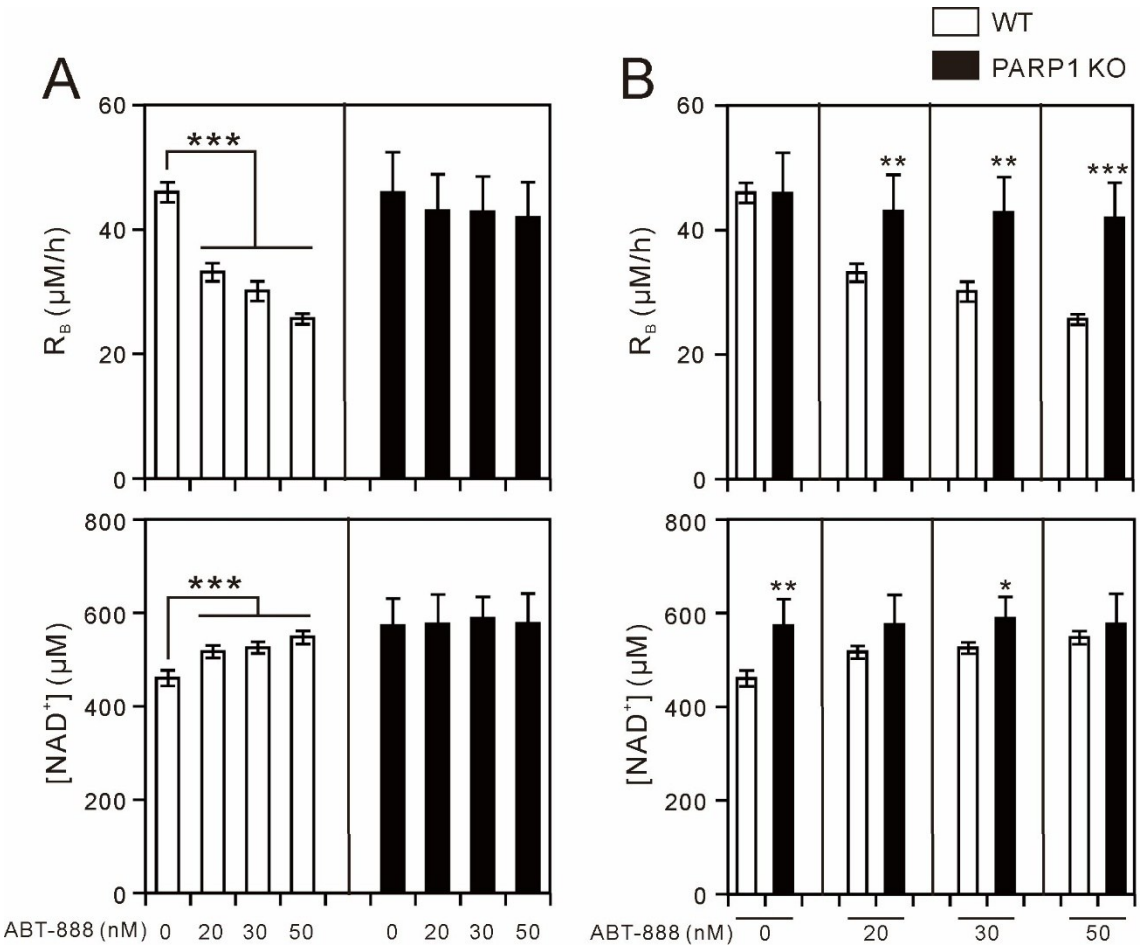
A
B
WT
PARP1 KO
R_B (μM/h)
[NAD$^+$] (μM)
***
**
*
ABT-888 (nM) 0 20 30 50 0 20 30 50
ABT-888 (nM) 0 20 30 50

Figure 7

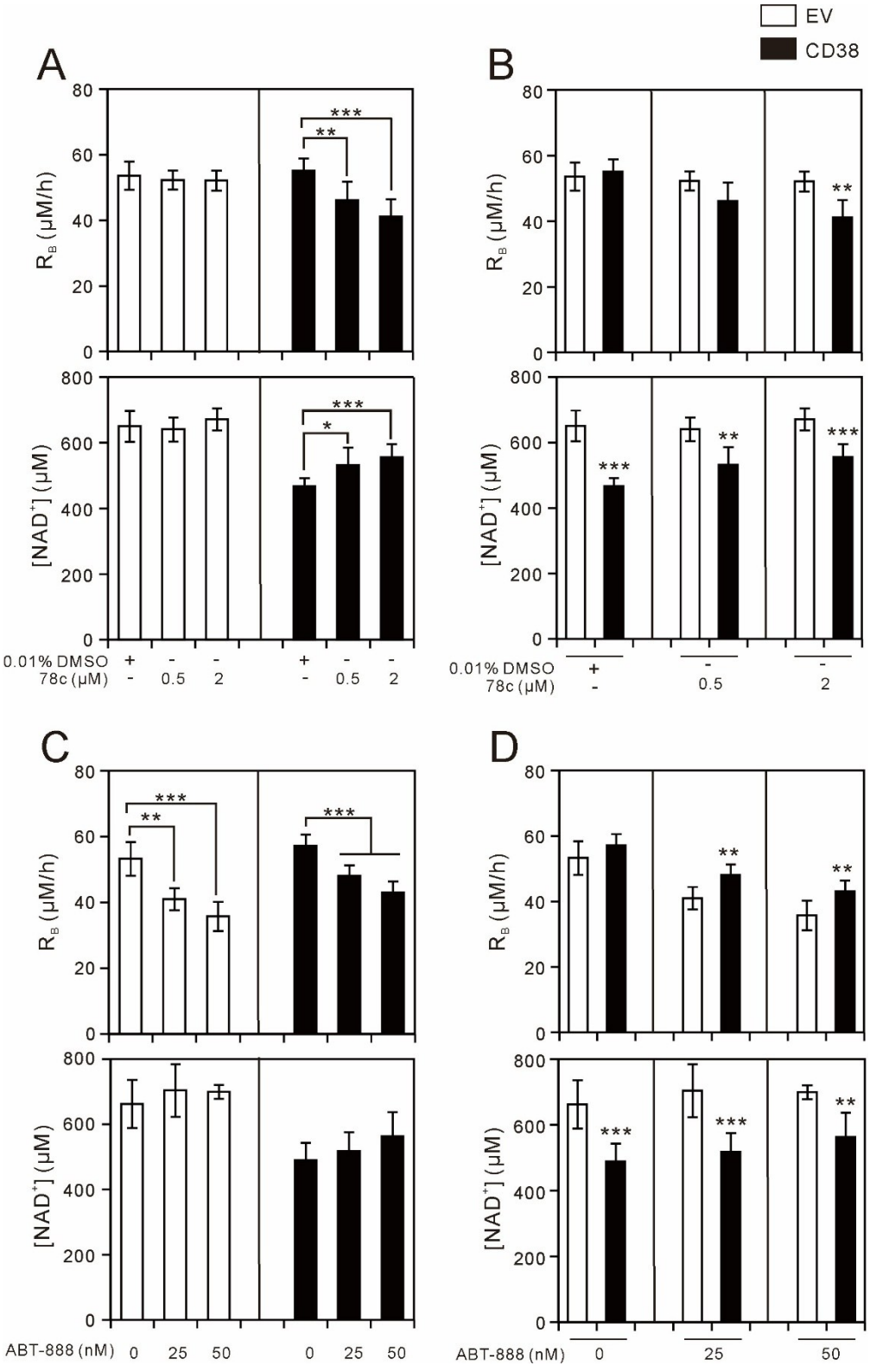

Figure 8

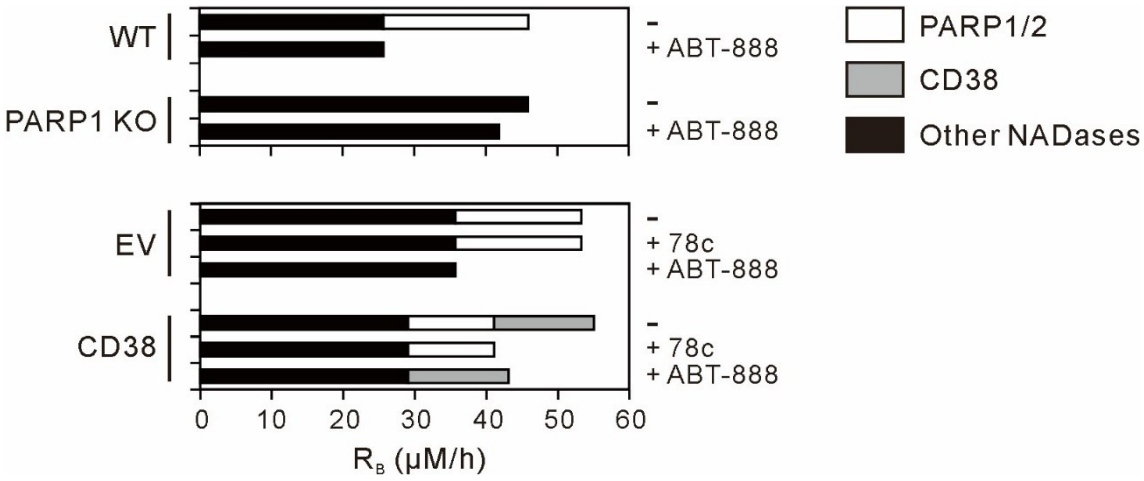

669

670

671 Figure 9